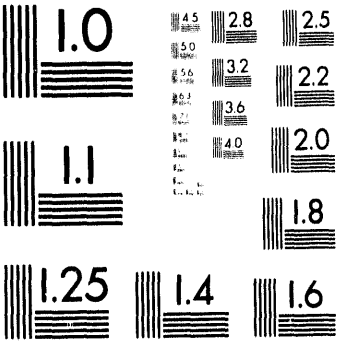
1.0
2.8
2.5
3.2
2.2
3.6
2.0
1.1
1.8
1.25
1.4
1.6

1 of 1

PREPARED FOR THE U.S. DEPARTMENT OF ENERGY,
UNDER CONTRACT DE-AC02-76-CHO-3073

PPPL-2938
UC-420,427

PPPL-2938

STABILITY OF THE TOROIDICITY-INDUCED ALFVÉN EIGENMODE IN AXISYMMETRIC TOROIDAL EQUILIBRIA

BY

G.Y. FU, C.Z. CHENG AND K.L. WONG

SEPTEMBER, 1993

PPPL PRINCETON PLASMA PHYSICS LABORATORY

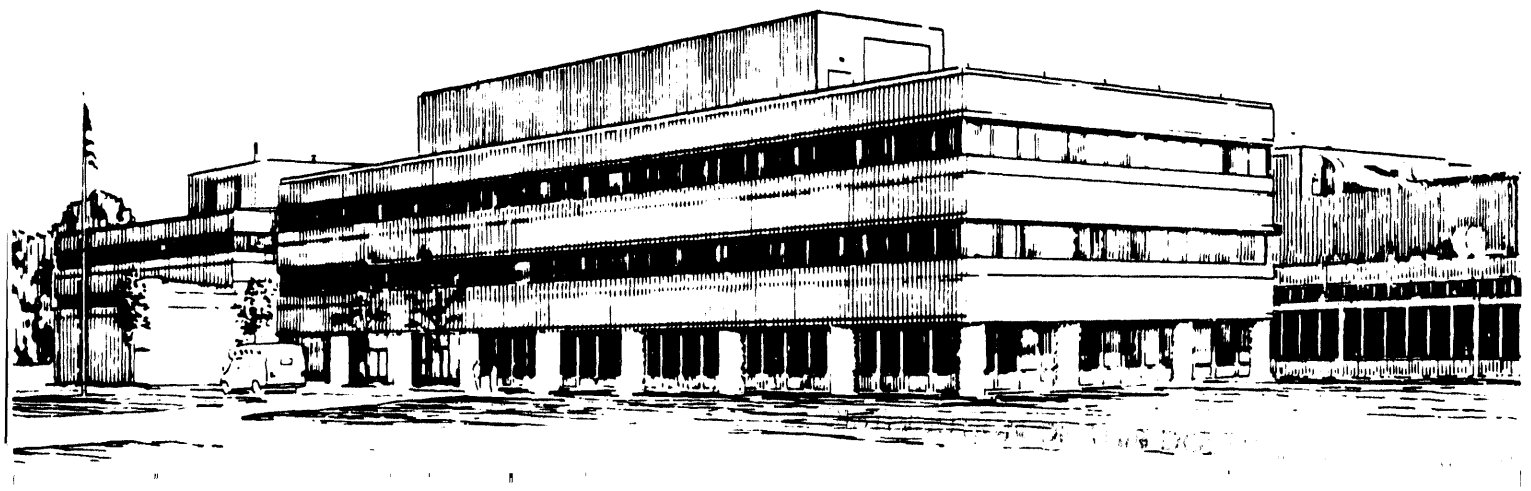

NOTICE

This report was prepared as an account of work sponsored by an agency of the United States Government. Neither the United States Government nor any agency thereof, nor any of their employees, makes any warranty, express or implied, or assumes any legal liability or responsibility for the accuracy, completeness, or usefulness of any information, apparatus, product, or process disclosed, or represents that its use would not infringe privately owned rights. Reference herein to any specific commercial produce, process, or service by trade name, trademark, manufacturer, or otherwise, does not necessarily constitute or imply its endorsement, recommendation, or favoring by the United States Government or any agency thereof. The views and opinions of authors expressed herein do not necessarily state or reflect those of the United States Government or any agency thereof.

NOTICE

This report has been reproduced from the best available copy.
Available in paper copy and microfiche.

Number of pages in this report: 54

DOE and DOE contractors can obtain copies of this report from:

Office of Scientific and Technical Information
P.O. Box 62
Oak Ridge, TN 37831;
(615) 576-8401.

This report is publicly available from the:

National Technical Information Service
Department of Commerce
5285 Port Royal Road
Springfield, Virginia 22161
(703) 487-4650

Stability of the Toroidicity-induced Alfvén Eigenmode in Axisymmetric Toroidal Equilibria

G. Y. Fu, C. Z. Cheng and K. L. Wong

Princeton Plasma Physics Laboratory

Princeton University, PO Box 451, Princeton, N. J. 08543

The stability of toroidicity-induced Alfvén eigenmodes (TAE) is investigated in general tokamak equilibria with finite aspect ratio and finite plasma beta. The finite orbit width of the hot particles and the collisional damping of the trapped electrons are included. For the trapped hot particles, the finite orbit width is found to be stabilizing. For the circulating hot particles, the finite orbit width effect is stabilizing for larger values of v_h/v_A (> 1) and destabilizing for smaller values of v_h/v_A (< 1), where v_h is the hot particle speed and v_A is the Alfvén speed. The collisional damping of the trapped electrons is found to have a much weaker dependence on the collision frequency than the previous analytic results. The contribution of the curvature term to the trapped electron collisional damping is negligible compared to that of the parallel electric field term for typical parameters. The calculated critical hot particle beta values for the TAE instability are consistent with the experimental measurements.

PACS number: 52.35.Bj, 52.55Fa

MASTER

DISTRIBUTION OF THIS DOCUMENT

I. INTRODUCTION

As we approach the realization of tokamak plasma ignition, it is crucial to understand the novel behaviors of burning plasma associated with energetic alpha particle in fusion reactors. In particular, the problem of toroidicity-induced shear Alfvén eigenmode[1,2] (TAE) destabilized by energetic alpha particles[3-5] has recently received a great deal of attention. It was pointed out in Ref. 1 and 2 that the TAE modes maybe destabilized by energetic particles through wave particle interaction. Fu[3], Fu and Van Dam[4], and Cheng, Fu and Van Dam[5] showed that the circulating alpha particles can strongly destabilize the n=1 TAE mode in an ignited tokamak. Much progress has since been made on understanding the energetic particle destabilizing effects on the TAE modes for both the low-n modes[6-12], and the high-n modes[13-15]. In particular, the important effects of finite orbit width of the energetic particles have been studied[11,15].

Recent experiments showed that TAE modes can be indeed destabilized by energetic circulating beam ions in the neutral beam injection (NBI) heated plasmas[16,17], and also by fast minority ions in the ion cyclotron radio frequency (ICRF) heated plasmas[18] and can lead to serious loss of energetic particles as shown in a numerical simulation[19]. However, the measured stability threshold was larger than that of the earlier works. Thus, it is required to include additional damping mechanisms, such as

ion Landau damping[8,9], the trapped electron collisional damping[20,21,15], the continuum damping[10,22-25], and the nonperturbative kinetic damping[26,27] due to coupling between magnetohydrodynamic (MHD) TAE mode and the kinetic Alfvén wave.

Most of previous studies made use of simplified large aspect ration, low beta plasma equilibria. On the other hand, a kinetic-MHD stability code[28] (NOVA-K) has been recently developed to calculate the stability of low-n TAE modes by properly taking into account the particle dynamics in general tokamak equilibria. A resistive MHD stability code[29] (NOVA-R) has also been developed to study the continuum damping effect for general tokamak equilibria. However, in the NOVA-K code, the effect of finite orbit excursion from the flux surface and the collisional damping of trapped electrons were neglected. In this work, we extend the kinetic-MHD model of Cheng[8,28] to include the effects of finite orbit width (FOW) of the hot particles due to the magnetic drift and the collisional damping due to trapped electrons for general tokamak equilibria. The FOW effect of the hot particles was studied previously for a model low-n TAE mode structure[11], and subsequently for high-n TAE modes using ballooning mode representation[15]. Here, we use the exact TAE mode structure in a general MHD equilibrium. Both the circulating hot particles and the trapped hot particles are included. Likewise, we calculate the trapped electron's collisional damping rigorously by numerically solving the bounce-averaged drift-kinetic equation

in general equilibria, without the usual approximation of model mode structures and boundary layer analysis[20,15].

We limit ourselves to a perturbative treatment of the kinetic effects. Thus, the non-perturbative kinetic damping of the TAE modes is beyond the scope of this work and is not considered here. The continuum damping is also not considered since the continuum damping is zero for the parameters and profiles used in this work. In another words, for the equilibria used here, the TAE mode frequency do not intersect with the Alfvén continuum. For other plasma parameters and profiles, the continuum damping may be present and can be calculated with the resistive MHD stability code such as NOVA-R[29].

The paper is organized as follows. In Section II, the formulation of this work is given. In Section III, the destabilizing contribution of the hot particles to the stability of TAE modes is calculated, including the FOW effects. The trapped electron collisional damping is considered in Section IV. In Section V, the stability threshold of the TAE modes is calculated and compared with the measurements in the Tokamak Fusion Test Reactor[30] (TFTR) experiments. In Section VI, the parameter dependence of the critical alpha particle beta is presented. Finally, the conclusions of this work is given in Section VII.

II. FORMULATION

A. Equations

We consider an axisymmetric toroidal plasma consisting of thermal electrons and thermal ions and a hot ion species. We start from the linearized momentum equation

$$\omega^2 \rho \xi = \nabla \delta P + \mathbf{B} \times \nabla \times \delta \mathbf{B} + \delta \mathbf{B} \times \nabla \times \mathbf{B}, \tag{1}$$

where ω is the mode frequency, ρ is the total plasma mass density, ξ is the usual fluid displacement, $\delta \mathbf{P}$ is the total perturbed pressure tensor due to all species, $\mathbf{B}$ and $\delta \mathbf{B}$ is the equilibrium and the perturbed magnetic field respectively. The following ideal MHD relation is assumed

$$\delta \mathbf{B} = \nabla \times (\xi \times \mathbf{B}). \tag{2}$$

The perpendicular electric field $\delta \mathbf{E}_\perp$ is expressed in terms of ξ

$$\delta \mathbf{E}_\perp = i\omega \xi \times \mathbf{B}. \tag{3}$$

Finally, the perturbed pressure tensor can be written in a diagonal form,

$$\delta \mathbf{P} = \delta P_\perp \mathbf{I} + (\delta P_\parallel - \delta P_\perp) \mathbf{bb}, \tag{4}$$

where the equilibrium is assumed to be isotropic, and $\delta P_\parallel$ and $\delta P_\perp$ are obtained from the perturbed particle distribution function δf as

$$\begin{pmatrix} \delta P_\parallel \\ \delta P_\perp \end{pmatrix} = \int d^3 v \delta f \begin{pmatrix} 2(\varepsilon - \mu B) \\ \mu B \end{pmatrix}, \tag{5}$$

where $\varepsilon = Mv^2/2$ is the particle energy, $\mu = Mv_\perp^2/2B$ is the magnetic moment and δf is given by

$$\delta f = -\xi_\perp \cdot \nabla F - \mu \frac{\delta B_\parallel}{B} \frac{\partial F}{\partial \varepsilon}(1 - \frac{\omega_*}{\omega})\Psi + g \tag{6}$$

with g being the solution of the drift-kinetic equation

$$(\frac{\partial}{\partial t} + v_\parallel \cdot \nabla + \mathbf{v}_d \cdot \nabla)g = ie\frac{\partial F}{\partial \varepsilon}(\omega - \omega_*)(\frac{i}{\omega}\mathbf{v}_d \cdot \delta \mathbf{E}_\perp + \Psi + \frac{\mu}{e}\delta B_\parallel). \tag{7}$$

In Eq. (6) and (7), $\delta B_\parallel$ is the parallel component of the perturbed magnetic field, Ψ is related to the perturbed parallel electric field $\delta E_\parallel = -\mathbf{b} \cdot \nabla \Psi$, $\mathbf{b}$ is the unit vector along the magnetic field lines, ω_* is the diamagnetic drift frequency, and $\mathbf{v_d}$ is the magnetic drift velocity. ω_* and $\mathbf{v_d}$ are defined as follows

$$\omega_* = \frac{i\mathbf{b} \times \nabla F \cdot \nabla}{M\omega_c \partial F/\partial \varepsilon}, \tag{8}$$

$$\mathbf{v}_d = \frac{\mathbf{b} \times (\mu \nabla B + Mv_\parallel^2 \kappa)}{M\omega_c}, \tag{9}$$

where ω_c is the particle cyclotron frequency and $\kappa = \mathbf{b} \cdot \nabla \mathbf{b}$ is the magnetic field line curvature.

It might be useful to add how the Eq. (7) is derived. Equation (7) is obtained from the standard drift-kinetic equation by using following relation:

$$\Phi - v_\parallel A_\parallel/c = \frac{i}{\omega}[\frac{\partial \Phi}{\partial t} + v_\parallel(\mathbf{b} \cdot \nabla \Phi + \delta E_\parallel)]$$

$$= \frac{i}{\omega}[\frac{d}{dt}(\Phi - \Psi) + \frac{\partial \Psi}{\partial t} - \mathbf{v}_d \nabla(\Phi - \Psi)]$$

$$\approx \frac{i}{\omega}[\frac{d}{dt}(\Phi - \Psi) - i\omega\Psi + \mathbf{v}_d \cdot \mathbf{E}_\perp] \tag{10}$$

where the perturbed electric field is expressed in terms of the electric potential Φ and the magnetic vector potential $\mathbf{A}$ as $\delta\mathbf{E} = -\nabla\Phi + \frac{1}{c}\frac{\partial \mathbf{A}}{\partial t}$, the parallel component of $\mathbf{A}$ is eliminated in favor of the parallel electric field potential Ψ, the perpendicular component of $\mathbf{A}$ is neglected for low beta plasmas, and the $\mathbf{v}_d \cdot \nabla\Psi$ term is also neglected, since both the drift velocity and the parallel potential is small. For MHD TAE modes, the parallel potential Ψ maybe calculated perturbatively using quasineutrality condition. Following Fu and Cheng[15], the potential Ψ satisfies following quasineutrality condition:

$$\sum_j \int d^3v q_j J_0 g_j = \sum_j \frac{n_j q_j^2}{T_j}\Psi + \sum_j \int d^3v (1 - J_0^2)\frac{q_j^2}{T_j} F_j(\Phi - \Psi). \tag{11}$$

where $J_0 = J_0(\nabla_\perp v_\perp/\omega_c)$ is the zeroth order Bessel function. It should be pointed out that J_0 contains finite Larmor radius effect (FLR) which is kept for the calculation of the parallel electric field. Elsewhere, the FLR effect will be neglected. Furthermore, we note that the non-adiabatic distribution function g_j is needed to obtain an explicit expression for Ψ. For shear Alfvén wave, the ordering of $k_\parallel v_i << \omega << k_\parallel v_e$ is appropriate, where v_i and v_e are thermal ion speed and thermal electron speed, respectively. Thus, the thermal ion contribution to the left hand side of Eq. (11) is much larger than the thermal electron contribution which can be neglected. The hot

particle contribution can also be neglected because the density of the hot species is much lower than that of thermal species. From Eq. (7), the leading order perturbed ion distribution is given by $g_i \approx \frac{eF_i}{T_i}(\frac{i}{\omega}\mathbf{v}_d \cdot \delta\mathbf{E}_\perp + \Psi)$. Plugging g_i into Eq. (11) and expanding the Bessel function to second order in ion Larmor radius, the leading order Ψ can then be expressed as

$$\Psi \approx \frac{1}{2}\rho_s^2 \nabla \cdot \delta\mathbf{E}_\perp - \frac{i}{\omega} < \mathbf{v}_{de} > \cdot \delta\mathbf{E}_\perp \tag{12}$$

where ρ_s is the ion Larmor radius defined with electron temperature, and $< \mathbf{v}_{de} >$ is the electron magnetic drift velocity averaged over the Maxwellian distribution of electrons. Equations (1-7, 12) constitute the kinetic-MHD model for the stability of the TAE modes. We note that various kinetic effects, such as hot particle destabilizing contribution and ion Landau damping, etc., are contained in the pressure tensor $\delta\mathbf{P}$ through g, which is the non-adiabatic part of the perturbed distribution function.

B. Quadratic Form

In order to calculate the kinetic effects perturbatively, we construct a quadratic form from the momentum equation. First, we separate the total perturbed pressure tersor into two parts: $\delta\mathbf{P} = \delta\mathbf{P}_f + \delta\mathbf{P}_k$, where $\delta\mathbf{P}_f$ is the fluid part which comes from the adiabatic response of δf, and $\delta\mathbf{P}_k$ is the kinetic part which comes from the non-adiabatic response g. Note that the $\delta\mathbf{P}_f$ can be expressed explicitly in terms of ξ as $\delta\mathbf{P}_f = -\xi \cdot \nabla P$ with P being the equilibrium pressure, assuming that the equilibrium

is isotropic. Now we take an inner product of Eq. (1) with ξ^* and integrate over the whole plasma volume to obtain a quadratic form

$$\delta W_f + \delta W_k - \omega^2 \delta K = 0, \tag{13}$$

where superscript $*$ denotes complex conjugate and

$$\delta K = \int d^3x \rho |\xi|^2, \tag{14}$$

$$\delta W_f = \int d^3x \xi^* \cdot [\nabla \cdot \delta \mathbf{P}_f + \delta \mathbf{B} \times \nabla \times \mathbf{B} + \mathbf{B} \times \nabla \times \delta \mathbf{B}], \tag{15}$$

$$\delta W_k = \int d^3x \xi^* \cdot \nabla \delta \mathbf{P}_k. \tag{16}$$

We remark that δK and δW_f comes from the ideal MHD equation, whereas δW_k represents the correction due to kinetic effects. With aid of Eq. (2-5), it can be easily shown that δW_k can be written more explicitly as

$$\delta W_k = -e \int d^3x \int d^3v (\frac{i}{\omega} \mathbf{v}_d \cdot \delta \mathbf{E}_\perp + \frac{\mu}{e} \delta B_\parallel)^* g. \tag{17}$$

Finally, we use the quasi-neutrality condition, i.e., $\sum_j e \int d^3v \delta f_j = 0$ with the subscript j denoting the particle species, to obtain an explicit quadratic form for δW_k

$$\begin{aligned} \delta W_k = 4i \int d^3x \int d^3v \varepsilon^2 \frac{\partial F}{\partial \varepsilon} (\omega - \omega_*) G^* (\frac{\partial}{\partial t} + v_\parallel \cdot \nabla + \mathbf{v}_d \cdot \nabla)^{-1} G \\ - \int d^3x \int d^3v e^2 \frac{\partial F}{\partial \varepsilon} |\Psi|^2, \end{aligned} \tag{18}$$

where the superscript -1 denotes the inversion of the propagator, and the function G is defined as

$$G = \frac{e}{2\varepsilon}(\frac{i}{\omega}\mathbf{v}_d \cdot \delta\mathbf{E}_\perp + \Psi + \frac{\mu}{e}\delta B_\parallel). \tag{19}$$

In deriving Eq. (18), we subtract and add Ψ in the parenthesis of Eq. (17), and then use the quasineutrality condition to eliminate $\int d^3v\Psi g$ term in favor of $\int d^3v\partial F/\partial\varepsilon|\Psi|^2$ term. We note that the inversion of the propagator can be accomplished by solving the drift-kinetic equation. This will be done in Sec. III for hot particles and in Sec IV for trapped electrons.

C. Perturbative Calculation of Kinetic Effects

Before going into detailed solutions of the drift-kinetic equation for each species, we first consider here the perturbative method used to calculate the kinetic effects. We assume that the kinetic effects are sufficiently small so that they do not change the basic ideal MHD mode structure. Our goal is to calculate the kinetic contribution to the eigenfrequency in order to determine the stability of the TAE modes. To this end, we expand the eigenfrequency and eigenfunction order by order in terms of a small parameter related to the weak kinetic effects. The zeroth order equation is then

$$\delta W_f(\xi_0^*, \xi_0) - \omega_0^2 \delta K(\xi_0^*, \xi_0) = 0, \tag{20}$$

which is just the ideal MHD energy principle. Here the subscript 0 denotes the zeroth

order. To the first order, we obtain

$$\delta W_f(\xi_0^*, \xi_1) - \omega_0^2 \delta K(\xi_0^*, \xi_1) - 2\omega_0\omega_1 \delta K(\xi_0^*, \xi_0) + \delta W_k(\xi_0^*, \xi_0, \omega_0) = 0. \tag{21}$$

The first two terms of Eq. (21) cancel due to the self-adjointness of the ideal MHD equation, and the remaining two terms yield a quadratic expression for the kinetic correction to the eigenfrequency

$$\frac{\omega_1}{\omega_0} = \frac{\delta W_k(\xi_0^*, \xi_0, \omega_0)}{2\omega_0^2 \delta K(\xi_0^*, \xi_0)}. \tag{22}$$

III. ENERGETIC PARTICLE CONTRIBUTION

Here, we compute the energetic particle contribution to δW_k. The derivation presented here extends the work of Cheng[8] to include the finite orbit width due to the magnetic drift. In the following, we will derive separately the circulating particle contribution and the trapped particle contribution, and then give numerical results.

A. Circulating Particle Contribution

To begin with, we solve Eq. (7) by integrating along the unperturbed particle orbit. For simplicity, we rewrite Eq. (7) as

$$\frac{d}{dt} g^\sigma = H(r, \theta, \phi, t) = \sum_m H_m(r, \theta) \exp[i(m\theta - n\phi - \omega t)] \tag{23}$$

where d/dt denotes the total time derivative along the unperturbed particle orbit, the function H is the right hand side of Eq. (7), σ is the sign of the parallel velocity, r

is the poloidal flux variable, θ and ϕ are the generalized poloidal and toroidal angles, respectively, and m and n are the poloidal and toroidal mode numbers respectively. In Eq. (23), we have expanded the function H in terms of poloidal Fourier components of the perturbed fields. Note that the poloidal dependence of $H_m(r,\theta)$ comes from the equilibrium quantities. The solution of Eq. (23) is then

$$g^{\sigma} = \int_{-\infty}^{t} \sum_{m} H_m(r',\theta') \exp[i(m\theta' - n\phi' - \omega t')]dt', \tag{24}$$

where $r' = r'(t')$, $\theta' = \theta'(t')$ and $\phi' = \phi'(t')$ are the trajectory of the unperturbed particle orbit with boundary conditions at $t' = t$: $r'(t) = r$, $\theta'(t) = \theta$ and $\phi'(t) = \phi$.

At this point, it is appropriate to determine the particle orbit in an equilibrium magnetic field of an axisymmetric tokamak. First, we note that the radial flux variable r is no longer a constant of motion due to the magnetic drift. Instead, the toroidal angular momentum P_ϕ is conserved, i.e.,

$$P_\phi = r - \frac{Mc}{e} v_\phi R = constant. \tag{25}$$

Thus, the orbit equation for r' is

$$r' = \bar{r} + \frac{Mc}{e}(v_{\|}R - < v_{\|}R >), \tag{26}$$

where $\bar{r} =< r >$, $<>$ denotes the averaging over the entire orbit. Also, we have used the parallel velocity $v_{\|}$ to approximate v_ϕ, the toroidal component of the particle

velocity. To continue, we define the instantaneous drift frequency ω_d to be

$$\omega_d = -n(\frac{d}{dt}\phi - \bar{q}\frac{d}{dt}\theta)$$

$$= -n[\mathbf{v_d} \cdot (\nabla\phi - \bar{q}\nabla\theta) + (q - \bar{q})v_{\parallel}\mathbf{b} \cdot \nabla\theta] \tag{27}$$

and make use of the following definitions:

$$S_m = m - n\bar{q}, \tag{28}$$

$$W(t) = \int_0^t dt'(\omega_d - < \omega_d >). \tag{29}$$

The exponent in Eq. (24) can now be written explicitly

$$m\theta' - n\phi' - \omega t' = (m\theta - n\phi - \omega t) - (\omega - < \omega_d > -\sigma S_m \omega_t (t' - t))$$

$$+[S_m(\theta' - \theta) - \sigma S_m \omega_t (t' - t) + W(t') - W(t)] \tag{30}$$

where $\omega_t = 2\pi/\tau_t$ is the transit frequency with τ_t being the transit period of the circulating particles. Note that the third term in Eq. (30) is a periodic function of t' with the period τ_t, and so is $H_m(r', \theta')$. Thus, we can make Fourier expansion in following manner:

$$H_m(r', \theta') \exp[i(S_m\theta' - \sigma S_m \omega_t t' + W(t'))] = \sum_p H^{\sigma}_{m,p} \exp(ip\omega_t t'), \tag{31}$$

where r' is given by Eq. (26), p is an integer to be summed from $-\infty$ to $+\infty$, and $H^{\sigma}_{m,p}$ is given by

$$H^{\sigma}_{m,p}(\bar{r}) = \frac{1}{\tau_t} \oint dt' H_m(r', \theta') \exp[i(S_m\theta' - (p\omega_t + \sigma S_m \omega_t)t' + W(t'))] \tag{32}$$

Equatin (24) can now be integrated to give

$$g^\sigma = \sum_{m,p} \frac{iH^\sigma_{m,p} \exp[i((p+\sigma S_m)\omega_t t^\sigma - S_m\theta - W(t))]}{\omega - <\omega_d> - (p+\sigma S_m)\omega_t} \exp[i(m\theta - n\phi - \omega t)] \quad (33)$$

where we have defined a time-like variable $t^\sigma(\theta)$

$$t^\sigma(\theta) = \sigma \int_0^\theta \frac{jB}{|v_{\|}|} d\theta. \quad (34)$$

It should be pointed out that the symmetry relation $H^\sigma_{m,p} = H^{-\sigma}_{m,-p}$ found in Ref. 8 is broken due to the finite orbit width, since r' depends on σ in Eq. (32). Given Eq. (33), the circulating particle contribution can be derived straightforwardly to obtain

$$\delta W_k = -\frac{8\pi^2}{M^2} \sum_{m',m}^{\sigma,p} \int d\bar{r} \int \frac{d\Lambda}{B} \varepsilon^3 d\varepsilon \tau_t(\omega - \omega_*) \frac{\partial F}{\partial \varepsilon} \frac{(G^\sigma_{m',p})^* G^\sigma_{m,p}}{\omega - <\omega_d> - \sigma(p+S_m)\omega_t}, \quad (35)$$

where $\Lambda = \mu B_0/\varepsilon$ is the pitch angle variable, and $G^\sigma_{m,p}$ is defined exactly the same way as $H^\sigma_{m,p}$, with function G in Eq. (19) replacing function H in Eq. (32). In the limit of zero orbit width, Eq. (35) reduces to Eq. (3.74) in Ref. 8.

B. Trapped Particle Contribution

The solution of Eq. (7) for trapped particle can be similarly derived, but some care must be taken of the fact that the trapped particle orbit samples only a part of a field line and that the parallel velocity changes sign at the turning points. The solution is

$$g^\sigma = \sum_{m,p} \frac{iH_{m,p} \exp[i(p\omega_b t^\sigma - S_m\theta - W(t))]}{\omega - <\omega_d> - p\omega_b} \exp[i(m\theta - n\phi - \omega t)], \quad (36)$$

where we have defined the time-like variable for trapped particles

$$t^+(\theta) = \int_0^\theta \frac{jB}{|v_\parallel|} d\theta \tag{37}$$

for $\tau_b/4 > t^+ > -\tau_b/4$ and $t^-(\theta) = \tau_b/2 - t^+(\theta)$ for $3\tau_b/4 > t^- > \tau_b/4$, and $H_{m,p}$ is given by

$$\begin{aligned} H_{m,p}(\bar{r}) &= \frac{1}{\tau_b} \oint dt' H_m(r', \theta') \exp[i(S_m\theta' - p\omega_b t' + W(t'))] \\ &= \sum_\sigma \frac{1}{\tau_b} \int_{-\theta_T}^{\theta_T} \frac{jBd\theta'}{|v_\parallel|} H_m(r'_\sigma, \theta') \exp[i(S_m\theta' - p\omega_b t^\sigma + W(t'))] \end{aligned} \tag{38}$$

where the subscript σ in r' denotes the sign of $v_\parallel$, and τ_b is the orbit period of the trapped particles. Note that $< v_\parallel R > \approx 0$ for trapped particles, thus $r'_\sigma = \bar{r} + \sigma Mc|v_\parallel|R/e$. The corresponding trapped particle contribution to δW_k is

$$\delta W_k = -\frac{8\pi^2}{M^2} \sum_{m',m}^{p} \int d\bar{r} \int \frac{d\Lambda}{B} \varepsilon^3 d\varepsilon \tau_b (\omega - \omega_*) \frac{\partial F}{\partial \varepsilon} \frac{(G_{m',p})^* G_{m,p}}{\omega - < \omega_d > -p\omega_b} \tag{39}$$

where $G_{m,p}$ is defined the same way as $H_{m,p}$ in Eq. (38). In the limit of zero banana width, Eq. (39) reduces to Eq. (3.72) of Ref. 8.

C. Numerical Results

Here, we present the numerical results for the FOW effects obtained by using Eq. (22), (35) and (39). Since we are interested in stability, we calculate only the resonant contribution of δW_k or the imaginary part of ω_1. We consider the parameters of the TFTR neutral beam injection (NBI) experiments[16]: the major radius $R = 240cm$, the

minor radius $a = 75cm$, the toroidal magnetic field $B = 1.0T$, the central temperature $T_i(0) = T_e(0) = 1.2kev$, the central plasma density $n_e(0) = 2.7 \times 10^{13}cm^{-3}$, the effective thermal ion mass $m_{eff} = 2.$, the effective charge $Z_{eff} = 2.5$, the beam particle mass $m_b = 2.0$, and beam injection energy $E_b = 110kev$. The plasma pressure profile is $P = P_0(1 - x^2)^{3/2}$, the density profile is $n_e = n_0(1 - 0.8x^4)$, where x is the square root of the normalized poloidal flux, the safety factor q is specified by four parameters as in Ref. 8, the central $q_0 = 1.0$, the edge $q_1 = 3.5$, $q_0' = 1.2$ and $q_1' = 3.5$, where the prime denotes the derivative with respect to the normalized poloidal flux. The beam density profile is $n_b = n_b(0)\exp[-(x/L_b)^2]$ with $L_b = 0.44$. Note that for this beam density profile, the absolute density scale length at $x = 0.5$ is $18cm$, which corresponds to the experimental measurement[16]. Finally the beam distribution function F_b is assumed to be a slowing-down with a single pitch angle, i.e., $F_b(\varepsilon, \Lambda) \propto \varepsilon^{-3/2}\delta(\Lambda - \Lambda_0)$ with $\Lambda_0 = 0$ for tangential injection.

Figure 1 shows the surface component of the MHD plasma displacement vector ξ of a $n = 2$ TAE mode as a function of radial variable x. A total of four poloidal harmonics are plotted. We note that the $m = 2$ and $m = 3$ harmonics dominate over others and peak at $x = 0.41$ where $q = 1.25$. It is instructive to compare the orbit width of the energetic beam particles with the radial mode width. the orbit width due to the magnetic drift can be derived from Eq. (25) and is on order of $\Delta_b = 2qv/\omega_c$.

For the parameters considered here, $\Delta_b = 16cm$ which is 1/5 of the minor radius and is somewhat larger than the radial mode width of Fig. 1. Therefore, we expect the FOW effects to be significant. This is confirmed in Fig. 2, which shows the growth rate of the same mode due to the circulating beam particles as a function of the ratio of the beam speed and the Alfvén speed. The solid line is calculated with the FOW effects and the dashed curve is obtained by turning off the FOW effects. We observe that the FOW effect is stabilizing for larger values of v_b/v_A, but it is destabilizing for smaller values of v_b/v_A due to the resonance broadening. This feature exhibits two opposite influences of FOW: on one hand, FOW is stabilizing due to the usual orbit averaging of the localized wave; on the other, FOW is destabilizing due to the resonance broadening. The same feature was previously found for the high-n TAE modes[15]. For the particular case considered in Fig. 2, the primary wave-particle resonance $v_{\|} \approx v_A$ is satisfied for $v_b/v_A > 1.15$ at $q = 1.25$ where the mode peaks and the effect of the orbit averaging is dominating; on the other hand, for smaller values of $v_b/v_A < 1.15$, the primary resonance is only satisfied away from where the mode peaks and the effect of the resonance broadening is dominating.

Figure 3 shows the growth rate of the $n = 2$ TAE mode due to the trapped beam particles with single pitch angle $\Lambda \approx 1.0$. We observe that the FOW effect is always stabilizing. For these parameters, the trapped particle contribution is reduced by

almost a factor of 10. It is instructive to note that the banana width of the trapped particles is on order of $50cm$ and is much larger than the mode width.

In summary, the finite orbit width effect can be either stabilizing or destabilizing for circulating particles, depending on the ratio of the hot particle speed and the Alfvén speed. For trapped particles, the FOW effect is found to be always stabilizing.

IV. COLLISIONAL DAMPING OF TRAPPED ELECTRONS

Here we consider the collisional damping of the TAE mode due to trapped electrons. Gorenlenkov and Sharapov showed that the dominant electron damping comes from the collisional trapped electrons[20]. Rosenbluthrosen included parallel electric field term, in addition to the curvature term considered in Ref. 20. Fu and Cheng[15] further showed that the contribution of the curvature term to the collisional damping vanishes as the real frequency of the TAE mode approaches the bottom edge of the continuum gap. All these previous results were obtained by solving the bounce-averaged drift-kinetic equation approximately as a boundary layer problem for a model TAE wave structure. In this work, we extend previous work to general equilibria by solving numerically the bounce-averaged drift-kinetic equation, which is

$$(-i\omega - < C >)g = < H >, \tag{40}$$

where $< C >$ is the bounce-averaged pitch angle scattering operator given by

$$< C >= 2\nu_e(\frac{\varepsilon}{T_e})^{-3/2}\frac{\Pi(\sqrt{\varepsilon/T_e})}{\int jB\frac{v}{v_\parallel}d\theta}\frac{\partial}{\partial\Lambda}(\Lambda\int jB\frac{v_\parallel}{v}d\theta)\frac{\partial}{\partial\Lambda} \tag{41}$$

with the function $\Pi(z)$ being defined as

$$\Pi(z) = Z_{eff} + \frac{1}{\sqrt{\pi}z}e^{-z^2} + \frac{1}{\sqrt{\pi}}(2 - \frac{1}{z^2})\int_0^z e^{-t^2}dt. \tag{42}$$

Here, ν_e is a normalized electron collision frequency and is given by $\nu_e = 4\pi n_e e^4 \ln(\Lambda_e)/(m_e^2 v_e^3)$, where n_e is electron's density, m_e is electron mass, v_e is electron thermal speed and $\ln(\Lambda_e)$ is the Coulomb logarithm. Note that in the left side of Eq. (40), we have neglected the drift term which is small for electrons. For convenience of solving Eq. (40), we make the change of variable $\eta^2 = (\Lambda_{max} - \Lambda)/(\Lambda_{max} - \Lambda_{min})$, where Λ_{min} and Λ_{max} is the lower bound and the upper bound of the pitch angle variable $\Lambda = \mu B_0/\varepsilon$ for trapped particles. Then, Eq. (40) becomes

$$[1 - iC_E\frac{1}{\tau_b\eta}\frac{\partial}{\eta}D(\eta)\frac{\partial}{\partial\eta}]g = \frac{i}{\omega} < H > \tag{43}$$

with

$$D(\eta) = \frac{\tau_b\Lambda}{\delta\Lambda} < 1 - \Lambda B >, \tag{44}$$

$$C_E = \frac{\nu_e/\omega}{2\delta\Lambda}(\frac{\varepsilon}{T_e})^{-3/2}\Pi(\sqrt{\varepsilon/T_e}), \tag{45}$$

where $\delta\Lambda = \Lambda_{max} - \Lambda_{min}$. The boundary conditions are $g'(1) = 0$ and $g(1) = 0$. We solve Eq. (43) by expanding g in terms of an orthogonal set of basis function g_l

defined as the eigenfunction of the collisional operator. Thus, g_l is the solution of the following equation with eigenvalue λ_l

$$\frac{1}{\tau_b \eta}\frac{\partial}{\partial \eta} D(\eta)\frac{\partial}{\partial \eta} g_l = -\lambda_l g_l, \tag{46}$$

where l is a positive integer with $l = 1$ denotes the smallest eigenvalue. Thus, we can write $g = \sum_l a_l g_l$ with the coefficient a_l determined by Eq. (43) and is given by

$$a_l = \frac{i \int_0^1 \eta \tau_b < H > g_l d\eta}{\omega(1 + iC_E \lambda_l) \int_0^1 \eta \tau_b g_l^2 d\eta}. \tag{47}$$

The collisional contribution to δW_k can be derived straightforwardly using Eq. (17) and (47) to give

$$\delta W_{k,c} = -\sum_{l=1}^{\infty} \frac{16\pi^2}{M^2}\frac{\delta\Lambda}{B}\int d\bar{r}\frac{\partial F}{\partial \varepsilon}\varepsilon^3 d\varepsilon \frac{|\int_0^1 \eta \tau_b < G > g_l d\eta|^2}{(1 + iC_E \lambda_l)\int_0^1 \eta \tau_b g_l^2 d\eta}. \tag{48}$$

Note that we have neglected ω_* term since $\omega_* << \omega$ for electrons. From Eq. (48), it is easy to show that the imaginary part of $\delta W_{k,c}$ is negative, which implies damping.

Before going into detailed numerical results, it is appropriate to discuss the relative contribution of the parallel electric field term and the curvature term in the function H (i.e , the right hand side of Eq. (40) or Eq. (10)). Recall that $H \approx ie\partial F/\partial\varepsilon(i\mathbf{v}_d \cdot \delta\mathbf{E}_\perp + \omega\Psi)$. We found numerically that the curvature term is usually much smaller in comparison with the parallel term. The numerically calculated collisional damping rate due to the curvature term alone agrees with that of the analytic results[15], i.e.,

the second term of Eq. (67) in Ref. 15. The smallness of the curvature term is due to the fact that the contributions of the two dominating poloidal harmonics of the TAE mode nearly cancel when the mode frequency is close to the bottom edge of the continuum gap. This near cancellation is manifested as the dependence on the mode frequency through the parameter λ in Eq. (67) of Ref. 15. For typical case, the mode frequency is near the bottom edge of the continuum gap and $\lambda^2 \sim 0.1$. As a result, the curvature contribution to the the collisional damping is reduced by an order of magnitude in comparison with that of the previous work[20]. This near cancellation in the curvature term can be shown more explicitly as follows. To begin with, recall that the TAE mode is localized radially near the continuum gap, where a pair of neighboring poloidal harmonics, m and $m+1$, dominate over the other harmonics (see Fig. 2, for example). Thus the curvature term $\mathbf{v}_d \cdot \delta\mathbf{E}_\perp \propto \xi \cdot \kappa \approx \xi_s \kappa_s$ comes mainly from the surface component of the plasma displacement vector (since the radial component $\xi_r \sim \epsilon\xi_s$ is much smaller than ξ_s). Recall that κ is the magnetic field line curvature. Now, ξ_s can be expanded explicitly as $\xi_s \approx \xi_s^m(r)\sin((m - nq)\theta) + \xi_s^{m+1}(r)\sin((m+1-nq)\theta)$ for its variation along the field line, exploiting the fact that only two harmonics are important. Near the continuum gap location where $q = (m+1/2)/n$, ξ_s reduces to $\xi_s \approx (\xi_s^{m+1}(r) - \xi_s^m(r))\sin(\theta/2)$. Looking at Fig. 1 and 4, we observe that the difference between $\xi_s^m(r)$ and $\xi_s^{m+1}(r)$ is small.

Numerical results show that this difference becomes even smaller as the TAE mode frequency approaches the bottom edge of the continuum gap (when the plasma beta increases). Therefore, the contributions of the two poloidal harmonics to the curvature term nearly cancel when the mode frequency is close to the edge. In Ref. 15, this cancellation was shown analytically in the high-n limit.

We now present numerical results for the collisional damping rate obtained from Eq. (22) and (48). Since the curvature term is usually much smaller than the parallel electric field term, we will only compare the numerical results and the analytic results for the parallel electric field term alone. We consider the parameters of the TFTR ICRF experiments[18]: $R = 260cm$, $a = 96cm$, $B = 3.26T$, $T_e(0) = T_i(0) = 4.5kev$, $n_e(0) = 4.8 \times 10^{13}cm^{-3}$, the effective mass $m_{eff} = 2.$, the effective charge $Z_{eff} = 2.5$, the pressure profile $P = P_0(1 - x^2)^2$, the density profile $n_e = n_e(0)(1 - 0.8x^{2.4})$, and the safety profile $q = \exp[\ln(q_1)x^2]$ with the edge $q = q_1 = 5.6$. Figure 4 shows four poloidal harmonics of the surface component of the MHD displacement vector as a function of the radial variable x for the $n = 2$ TAE mode. This eigenmode is computed for the equilibrium considered here and is similar to that of Fig. 1. Figure 5 shows the collisional damping rate as a function of the normalized effective collisional frequency ν_{eff}/ω for the corresponding $n = 2$ eigenmode, where $\nu_{eff} = 2Z_{eff}\nu_e/\delta\Lambda$ evaluated at $x = 0.35$. The solid curve shows the analytic results obtained from Eq. (67) of Ref.

15 and the circle line is obtained numerically using Eq. (48). We see that, for small collisional frequency of $\nu_{eff}/\omega < 10^{-1}$, our numerical damping rate exhibits nearly the same scaling with ν_{eff}/ω and is about a factor of two smaller as compared to the analytic result. This difference of a factor of two is reasonable considering that how many approximations have been made in obtaining the analytic results[15]. However, for not very small collisional frequency of $\nu_{eff}/\omega > 10^{-1}$, the dependence of the collisional damping rate on the collisional frequency is much weaker for the numerical results than for the analytic one. This is due to the factor that the analytic scaling is only valid for very small ν_{eff}/ω. For typical parameters, the collisional frequency ranges from $\nu_{eff}/\omega \sim 10^{-1}$ for the TFTR ICRF experiments[18] to $\nu_e/\omega \sim 1$ for the TFTR NBI experiments[16]. This indicates that a numerical calculation of the collisional drift kinetic equation must be employed to obtain an accurate collisional damping rate due to the trapped electrons.

Before ending this section, it is instructive to discuss the convergence of the collisional damping rate with the number of the basis functions g_l. The first four eigenfunctions g_l are shown in Fig. 6 for the parameter of Fig. 5. For the range of ν_e/ω considered here, we find that a summation up to $l = 8$ is sufficient for good convergence. This result is not surprising, since we expected the convergence to occur when $C_E\lambda_l \sim O(1)$ or $l^2\nu_{eff}/\omega \sim O(1)$. Note that the eigenvalue is roughly $\lambda_l \sim l^2$. Then

we would expect a number of $l \sim 6$ is needed for convergence for $\nu_{eff}/\omega \sim 3 \times 10^{-2}$.

V. STABILITY THRESHOLD: COMPARISON WITH TFTR EXPERIMENTS

Here, we calculate the critical hot particle beta for the TAE instability by balancing the hot particle destabilizing contribution against ion Landau damping, electron Landau damping and trapped electron collisional damping.

A. The TFTR NBI Experiments

We consider the TFTR NBI experiments by Wong et al.[16] in which the $n = 2$ and $n = 3$ TAE modes were excited by the tangentially injected neutral beam ions. The parameters and profiles are given in Sec. III. The beam particle driven growth rates are given in Fig. 2 for the $n = 2$ mode. The ratio of beam particle speed and Alfvén speed is $v_b/v_A = 1.1$ for the plasma density of $n_e(0) = 2.7 \times 10^{13} cm^{-3}$. Thus, the finite orbit width effect is destabilizing. The FOW effect is also destabilizing for the $n = 3$ mode. Table I lists the critical beam beta values at the radius $x = 0.4$ for the $n = 1$, $n = 2$ and $n = 3$ TAE modes. We see that the calculated critical beam beta values agree well with the experimental measurements. It is instructive to compare the sie of various damping mechanisms. For the $n = 2$ mode, the ion Landau damping is comparable to the electron's collisional damping. For the $n = 3$ mode, the electron collisional damping is much larger than the ion Landau damping.

The electron Landau damping is negligible for both modes. It should be pointed out that both the FOW effect of the beam particle and the trapped electron collisional damping are crucial for good agreement between the theory and the experiment. Without these two effects, the predicted threshold would be a factor of five lower than the experimental measurement for the $n = 3$ mode. Finally, it should also be pointed out that the hot particle contribution is sensitive to the pitch angle, at least for the parameters considered here. We find that the hot particle drive increases by a factor of six when the pitch angle varies from $\Lambda = 0$ to $\Lambda = 0.75\Lambda_{min}$. This large change comes from the pitch angle dependence of the parallel wave-particle resonance condition, $\omega =< \omega_d > +k_{||}v_{||}$, where the transit averaged magnetic drift frequency $< \omega_d >$ is not zero for passing particles due to toroidicity and magnetic shear. For the parameters considered here, the primary resonance $v_A \approx< \omega_d > /k_{||} + v_{||}$ is not satisfied at the mode peak. Thus, the main hot particle contribution comes from the sideband resonance, $v_A \approx< \omega_d > /k_{||} + 3v_{||}$. This sideband resonance increases strongly as Λ increases. Therefore, one should be very careful in chosing the fast particle pitch angle distribution. Here, we use a single pitch angle at $\Lambda = 0$ for simplicity. In reality, the pitch angle distribution has a finite spread even for the case of parallel injection of neutral beam particles. In this case, the calculated critical beam beta would be somewhat higher.

B. The TFTR ICRF experiments

Here, we consider the TFTR ICRF experiments[18] in which the TAE modes were excited by the fast minority ions heated by ICRF. Some parameters and profiles for the core plasma have been given in Sec. IV. The fast ion distribution is chosen to be a Maxwellian with single pitch angle $\Lambda_0 = 1.0$ and The profile of the fast ion temperature is chosen to be $T_h = T_h(0)(1 - 2x/L_h + x^2/L_h^2)$ for $x < L_h$ and $T_h = 0$ for $x > L_h$, where $T_h(0) = 500kev$ and the radial scale length $L_h = 0.55$ corresponding to 40% of the whole minor radius. The fast ion density profile is assumed to be constant. Our choice of the fast particle distribution may be justified as follows. First, the energy distribution of the fast particles heated by ICRF is approximately Maxwellian due to balance between the ICRF heating and slowing down by electron collision, as shown by Stix[31]. Second, the fast particles are heated predominantly in the perpendicular direction during the ICRF heating. Furthermore, the ICRF heating is very localized near the magnetic axis. Thus the corresponding pitch angle of the fast particles is approximately $\Lambda = 1.0$. Table II lists the critical volume-averaged fast ion beta values for the $n = 2$ and the $n = 3$ TAE modes. We see that the calculated stability threshold agrees well with the experiment for the $n = 3$ mode, but for the $n = 2$ mode, the theoretical critical beta is about a factor of three lower than the experimental value. We find that for both modes, the trapped

electron collisional damping is the dominating damping mechanism. The ion Landau damping is negligible due to low thermal ion beta. Several reasons may be speculated to explain the discrepancy between the theory and the experiment for the $n = 2$ mode. First, some additional damping mechanisms which are neglected here may be important, such as the non-perturbative kinetic damping. Second, we find that the calculated fast ion drive is quite sensitive to the fast ion temperature and it's profile. For example, raising the central ion temperature from $500kev$ to $700kev$ would reduce the fast ion contribution by a factor of 2.2, and changing the temperature profile to $T_h = T_h(0)(1 - x/L_h)$ would reduce the fast ion drive by a factor of 7.7 ! Therefore, one needs an accurate experimental measurement of the fast ion parameter and profile to make a more conclusive calculation of the fast ion contribution. All these issues must be dealt with before a better comparison between theory and experiment can be made.

VI. PARAMETER DEPENDENCE OF STABILITY THRESHOLD IN AN IGNITED TOKAMAK

Here, we study the parameter dependence of the critical alpha beta for TAE stability in an ignited tokamak. We consider following parameters: the major radius $R = 250cm$, the minor radius $a = 80cm$, the toroidal magnetic field $B = 5T$, the central electron temperature $T_e(0) = 10kev$, the ion temperature $T_i(0) = 20kev$, the effective

ion mass $m_{eff} = 2.5$, the effective charge $Z_{eff} = 2.5$. The plasma pressure profile is $P = P_0(1 - x^2)^2$, the density profile $n_e = n_0(1 - 0.8x^2)$, where x is the square root of the normalized poloidal flux, the safety factor q is specified by four parameters as in Ref. 8, $q_0 = 1.1$, $q_1 = 5.5$, $q_0' = 1.0$ and $q_1' = 5.5$, where the prime denotes the derivative with respect to the normalized poloidal flux. The alpha particle density is given by $n_\alpha = n_\alpha(0)\exp(-x^2/L_\alpha^2)$, where L_α is the normalized density scale length. The alpha particle distribution function is assumed to be a slowing-down in energy and uniform in pitch angle. It should be noted that these parameters and profiles are similar to those expected in the planned TFTR D-T experiments[32]. For these parameters, the trapped electron collisional damping is very small. On the other hand, the FOW effect is important and will be discussed below.

A. Dependence on v_α/v_A

Figure 7 shows the critical volume-averaged alpha particle beta values as a function of v_α/v_A for the $n = 1$ TAE mode, where v_α is the fusion alpha particle speed at birth and v_A is the Alfvén phase speed evaluated at the magnetic axis. The solid dots in Fig. 7 are computed with the finite orbit width (FOW) effects of alpha particles due to the magnetic drift, whereas the circles are computed without FOW effects. A similar plot for the $n = 2$ mode is shown in Fig. 8. In these figures, we vary v_α/v_A by varying the plasma density while keeping all other parameters fixed. Since the

equilibrium beta is proportional to density, each dot (or circle) is computed with the self-consistent equilibrium at the corresponding beta value. We see that the FOW effects are stabilizing for larger values of v_α/v_A and destabilizing otherwise. The minimum of $< \beta_\alpha >$ occurs at $v_\alpha/v_A \approx 1.0$. The critical beta increases rapidly as v_α/v_A increases for $v_\alpha/v_A > 1.0$ due to increasing ion Landau damping. On the other hand, for $v_\alpha/v_A < 1.0$, the critical alpha beta increases as v_α/v_A decreasing due to increasing electron Landau damping and weakening alpha particle drive. For value of $v_\alpha/v_A \approx 1.4$ corresponding to the TFTR D-T experiments[32], the critical alpha beta is $< \beta_\alpha > \approx 6 \times 10^{-4}$, which is close to the expected alpha particle production in the TFTR D-T experiments.

B. Dependence on equilibrium beta

The results just shown in Fig. 7 and 8 are obtained with self-consistent equilibrium at finite plasma beta. Here, we show what will result if the zero beta equilibrium is used. Figure 9 compares the critical alpha beta values obtained using the self-consistent equilibria (solid dots) with that of zero beta equilibrium (circles) for the $n = 1$ mode. As expected, for small values of equilibrium beta or v_α/v_A, the critical alpha beta values are nearly the same for the two cases. However, for the larger values of v_α/v_A, the critical alpha beta with zero beta equilibria is much smaller than that with finite beta equilibria. We find this large difference comes mainly from the

dependence of the real mode frequency on the equilibrium beta. As the equilibrium beta increases, the real frequency becomes smaller. As a result, the ion Landau damping is enhanced strongly by the finite beta effects. On the other hand, the alpha particle drive is found not sensitive to the equilibrium beta. Thus, the critical alpha beta is enhanced by the finite equilibrium beta effects for $v_\alpha/v_A > 1.1$. (For $v_\alpha/v_A < 1.1$, the critical alpha beta is enhanced slightly by the finite equilibrium beta due to the increased electron Landau damping).

C. Dependence on T_i/T_e

Figure 10 shows the critical alpha beta of the $n = 1$ TAE mode as a function of the ratio of ion temperature and electron temperature for $T_i + T_e = 30keV$ and $v_\alpha/v_A = 1.38$. We see that $< \beta_\alpha >$ increases rapidly as T_i/T_e increases. This strong dependence is due to the fact that the ion Landau damping is sensitive to the ion beta. For the parameters considered here, the ion Landau damping is found to be the dominating damping mechanism.

D. Dependence on alpha particle density scale length

Figure 11 shows the critical alpha beta as a function of the alpha density scale length L_α with FOW effects (solid dots) and without FOW effects (circles) for the $n = 1$ TAE mode. Recall that the alpha density profile is chosen as $n_\alpha = n_\alpha(0)\exp(-x^2/L_\alpha^2)$,

where x is the square root of the normalized poloidal flux and L_α is the normalized alpha density scale length. In Fig. 11, we see that the critical alpha beta increases as L_α increases for both cases. The effects of FOW enhances the dependence of alpha critical beta on L_α, especially near $L_\alpha = 0.3$. This can be understood physically as follows. The dependence of alpha particle drive on L_α comes from the combination of two opposite effects. For smaller L_α, the destabilizing pressure gradient term is larger. However, the location of the largest pressure gradient of the alpha particles is further away from where the mode peaks. This shift of maximum gradient surface as L_α becomes smaller, which is stabilizing, is weaken by the FOW effects. As a result, the critical alpha beta is more sensitive to L_α with FOW effects than without FOW effects.

VII. CONCLUSIONS

We have presented a comprehensive analysis of the stability of the TAE modes in general tokamak equilibria, including the finite orbit width of the hot particles due to the magnetic drift and the collisional damping of trapped electrons, in addition to the Landau damping of the thermal ions and electrons. For the trapped hot particles, the finite orbit width is found to be stabilizing. For the circulating hot particles, the finite orbit width effect is stabilizing for larger values of v_h/v_A and destabilizing for smaller values of v_h/v_A. The collisional damping of trapped electrons is found to

have a much weaker dependence on the collision frequency than the previous analytic results for $\nu_{eff}/\omega > 10^{-1}$. The contribution of the curvature term to the collisional damping is negligible compared to that of the parallel electric field term for typical parameters. The calculated stability thresholds agree reasonably well with the TFTR experiments.

ACKNOWLEDGMENT

One of the author (G. Y. Fu) acknowledge Z. Chang, C. Philips and R. Wilson for providing the TFTR experimental data used in this paper and for valuable discussions. This work was supported by the U. S. Department of Energy Contract No. DE-AC02-76-CHO-3073.

REFERENCES

[1]C. Z. Cheng, L. Chen, and M. S. Chance, Ann. Phys. (N. Y.) **161**, 21 (1985).

[2]C. Z. Cheng and M. S. Chance, Phys. Fluids **29**, 3695 (1986).

[3]G. Y. Fu, Ph. D. Thesis, The University of Texas at Austin (1988).

[4]G. Y. Fu and J. W. Van Dam, Phys. Fluids **B1**, 1949 (1989).

[5]C. Z. Cheng, G. Y. Fu, and J. W. Van Dam, in Theory of Fusion Plasmas 1988, ed. J. Vaclavik, F. Troyon, and E. Sindoni (Societa Italiana di Fisica/Editrice Compositori, Bologna, Italy, 1989), p. 259.

[6]C. Z. Cheng, Fusion Technology **18**, 443 (1990).

[7]J. W. Van Dam, G. Y. Fu, and C. Z. Cheng, Fusion Technology **18**, 461 (1990).

[8]C. Z. Cheng, Phys. Fluids, **B3**, 2463 (1991).

[9]R. Betti and J. P. Freidberg, Phys. Fluids **B3**, 1865 (1991).

[10]H. L. Berk, J. W. Van Dam, Z. Guo, and D. M. Lindberg, Phys. Fluids **B4**, 1806 (1992).

[11]H. L. Berk, B. N. Breizman, and H. Ye, Phys. Lett. **A162**, 475 (1992).

[12]C. Z. Cheng, G. Y. Fu, H. E. Mynick, R. Budny, R. B. White, S. J. Zweben, C. T. Hsu, D. J. Sigmar, D. A. Spong, B. A. Carreras, and C. L. Hedrick, Proceedings of the Fourteen International Conference on Plasma Physics and Controlled Nuclear Fusion Research, Wurzburg, Germany, September, 1992 (International Atomic Energy Agency), IAEA-CN-56/D-2-1-1(c).

[13]L. Chen, in Ref. 5, p.327.

[14]D. A. Spong, J. A. Holmes, J. -N. Leboeuf, and P. J. Christenson, Fusion Technology **18**, 496 (1990).

[15]G. Y. Fu and C. Z. Cheng, Phys. Fluids B4, 3722 (1992).

[16]K. L. Wong, R. J. Fonck, S. F. Paul, D. R. Roberts, E. D. Fredrickson, R. Nazikian, H. K. Park, M. Bell, N. L. Bretz, R. Budny, S. Cohen, G. W. Hammett, F. C. Jobes, D. M. Meade, S. S. Medley, D. Mueller, Y. Nagayama, D. K. Owens, and E. J. Synakowski, Phys. Rev. Lett. **66**, 1874 (1991).

[17]W. W. Heidbrink, E. J. Strait, E. Doyle, G. Sager, and R. Snider, Nucl. Fusion **31**, 1635 (1991).

[18]J. R. Wilson, M. G. Bell, H. Biglari, M. Bitter, N. L. Bretz, R. Budny, C. E. Bush, L. Chen, Z. Chang, D. Darrow, P. C. Efthimion, E. Fredrickson G. Y. Fu, R. Goldfinger, B. Grek, L. R. Grisham, G. Hammett, R. J. Hawryluk, D. Hoffman,

J. C. Hosea, A. Janos, D. Jassby, F. C. Jobes, D. W. Johnson, L. C. Johnson, J. Machuzak, R. Majeski, D. K. Mansfield, E. Mazzucato, K. M. McGuire, S. S. Medley, D. Mueller, M. Mukarami, R. Nazikian, D. K. Owens, H. Park, S. Paul, C. K. Philips, A. T. Ramsey, D. Rasmussen, F. Rimini, J. H. Rogers, A. L. Roquemore, G. Schilling, J. Schivell, G. L. Schmidt, J. Stevens, B. C. Stratton, J. D Strachan, E. Synakowsi, G. Taylor, M. Ulrickson, K. L. Wong, M. Yamada, K. M. Young, M. C. Zarnstoff, and S. J. Zweben, in Ref. 12, IAEA-CN-56/E-2-2.

[19]D. J. Sigmar, C. T. Hsu, R. White, and C. Z. Cheng, Phys. Fluids B4, 1506 (1992).

[20]N. N. Gorelenkov and S. E. Sharapov, Physica Scripta, 45 (1991).

[21]M. N. Rosenbluth (private communication, 1992)

[22]F. Zonca and L. Chen, Phys. Rev. Lett., **68**, 592(1992)

[23]M. N. Rosenbluth, H. L. Berk, D. M. Lindberg, and J. W. Van Dam, Phys. Rev. Lett., **68**, 596 (1992).

[24]S. Poedts, W. Kerner, J. P. Goedbloed, B. Keegan, G. T. A Huysmans, Plasma Physics and Controlled Fusion, **34**, 1397 (1992)

[25]L. Villard and G. Y. Fu, Nucl. Fusion **32**, 1695 (1992).

[26]R. Mett and S. Mahajan, Phys. Fluids B 4, 2885 (1992).

[27]M. S. Chu, A. D. Turnbull, J. M. Greene, L. L. Lao, M. S. Chance, H. L. Berk, B. N. Breizman, W. Q. Li, D. M. Lindberg, S. M. Mahajan, R. R. Mett, D. W. Ross, J. W. Van Dam, H. Ye, J. Candy, M. N. Rosenbluth, Proceedings of the Fourteen International Conference on Plasma Physics and Controlled Nuclear Fusion Research, Wurzburg, Germany, September, 1992 (International Atomic Energy Agency), IAEA-CN-56/D-2-2.

[28]C. Z. Cheng, Phys. Reports **211**, 1 (1992).

[29]T. R. Harley, C. Z. Cheng, and S. C. Jardin, J. Comput. Phys., **103**, 43 (1992).

[30]D. M. Meade, V. Arunasalam, C. W. Barns, M. G. Bell, R. Bell, M. Bitter, R. Boivin, N. L. Bretz, R. Budny, C. E. Bush, A. Cavallo, C. Z. Cheng, T. K. Chu, S. A. Cohen, S. Cowley, S. Davis, D. L. Dimock, J. Dooling, H. F. Dylla, P. C. Efthimion, A. B. Ehrhardt, R. J. Fonck, E. Fredrickson, H. P. Furth, R. Goldston, G. Greene, B. Grek, L. R. Grisham, G. Hammett, R. J. Hawryluk, K. W. Hill, J. C. Hosea, R. B. Howell, R. A. Hulse, H. Hsuan, A. Janos, D. Jassby, F. C. Jobes, D. W. Johnson, R. Kaita, S. Kaye, J. Kesner, C. K. Phillips, S. J. Kilpatrick, H. Kugel, P. H. LaMarche, B. LeBlanc, D. M. Manos, D. K. Mansfield, E. S. Marmar, E. Mazzucato, M. P. McCarthy, M. Mauel, D. C. McCune, K. M. McGuire, S. S. Medley, D. R. Mikkelsen, D. Monticello, R. Motley, D. Mueller, J. Murphy, Y. Nagayama, G. A. Navratil, R. Nazikian, D. K. Owens, H. Park, S. Paul, R. Perkins,

S. Pitcher, A. T. Ramsey, M. H. Redi, G. Gewoldt, D. Roberts, A. L. Roquemore, P. H. Rutherford, S. Sabbagh, G. Schilling, J. Schivell, G. L. Schmidt, S. D. Scott, J. Snipes, J. Stevens, J. D. Strachan, B. C. Stratton, W. Stodiek, E. Synakowski, W. Tang, G. Talor, J. Terry, J. R. Timberlake, H. H. Towner, U. Ulrickson, S. von Goeler, R. Wieland, W. Williams, J. R. Wilson, K. L. Wong, M. Yamada, S. Yoshikawa, M. Young, M. C. Zarnstoff, and S. J. Zweben, Proceedings of the Thirteenth International Conference on Plasma Physics and Controlled Nuclear Fusion Research, Washington, DC, (International Atomic Energy Agency, Vienna, 1991), Vol. 1, p. 9.

[31]T. H. Stix, Nucl. Fusion **15**, 737 (1975)

[32]R. V. Budny, M. G. Bell, H. Biglari, M. Bitter, C. E. Bush, C. Z. Cheng, E. D. Fredrickson, B. Grek, K. W. Hill, H. Hsuan, A. C. Janos, D. L. Jassby, D. W. Johnson, L. C. Johnson, B. LeBlank, D. C. McCune, D. R. Mikkelsen, H. K. Park, A. T. Ramsey, S. A. Sabbagh, S. D. Scott, J. F. Schivell, J. D. Strachan, B. C. Stratton, E. J. Synakowski, G. Taylor, M. C. Zarnstorff, S. J. Zweben, Nucl. Fusion **32**, 429 (1992).

TABLE I. Comparison of the theoretical critical beam ion beta with the experimental measurements in the TFTR NBI-heated plasmas

critical beta	$n = 1$	$n = 2$	$n = 3$
$(\beta_h)_{exp}$	stable	0.5%	0.5%
$(\beta_h)_{theory}$	1.2%	0.47%	0.38%

TABLE II. Comparison of the theoretical critical fast ion beta with the experimental measurements in the TFTR ICRF-heated plasmas

critical beta	$n = 2$	$n = 3$
$< \beta_h >_{exp}$	2.7×10^{-4}	2.7×10^{-4}
$< \beta_h >_{theory}$	0.74×10^{-4}	3.5×10^{-4}

FIGURE CAPTIONS

Figure 1. The surface component of the MHD plasma displacement vector as a function of the radial variable x for the $n = 2$ TAE mode in the TFTR NBI experiment.

Figure 2. The circulating beam particle driven growth rates of the $n = 2$ TAE mode versus the ratio of the beam particle speed and the Alfvén speed with and without the finite orbit width effects.

Figure 3. The trapped beam particle driven growth rates of the $n = 2$ TAE mode versus the ratio of the beam particle speed and the Alfvén speed with and without the finite orbit width effects.

Figure 4. The surface component of the MHD plasma displacement vector as a function of the radial variable x for the $n = 2$ TAE mode in the TFTR ICRF experiment.

Figure 5. The collisional damping rate due to trapped electrons as a function of the effective collisional frequency.

Figure 6. The first four eigenfunctions of the collisional operator.

Figure 7. The critical volume-averaged alpha particle beta as a function of v_α/v_A for the $n = 1$ TAE mode with the FOW effects (solid dots) and without the FOW effects (circles).

Figure 8. The critical volume-averaged alpha particle beta as a function of v_α/v_A for the $n = 2$ TAE mode with the FOW effects (solid dots) and without the FOW effects (circles).

Figure 9. The critical volume-averaged alpha particle beta as a function of v_α/v_A for the $n = 1$ TAE mode obtained with self-consistent finite beta equilibria (solid dots) and the zero beta equilibrium (circles).

Figure 10. The critical volume-averaged alpha particle beta as a function of T_i/T_e for the $n = 1$ TAE mode.

Figure 11. The critical volume-averaged alpha particle beta as a function of the alpha density scale length L_α for the $n = 1$ TAE mode.

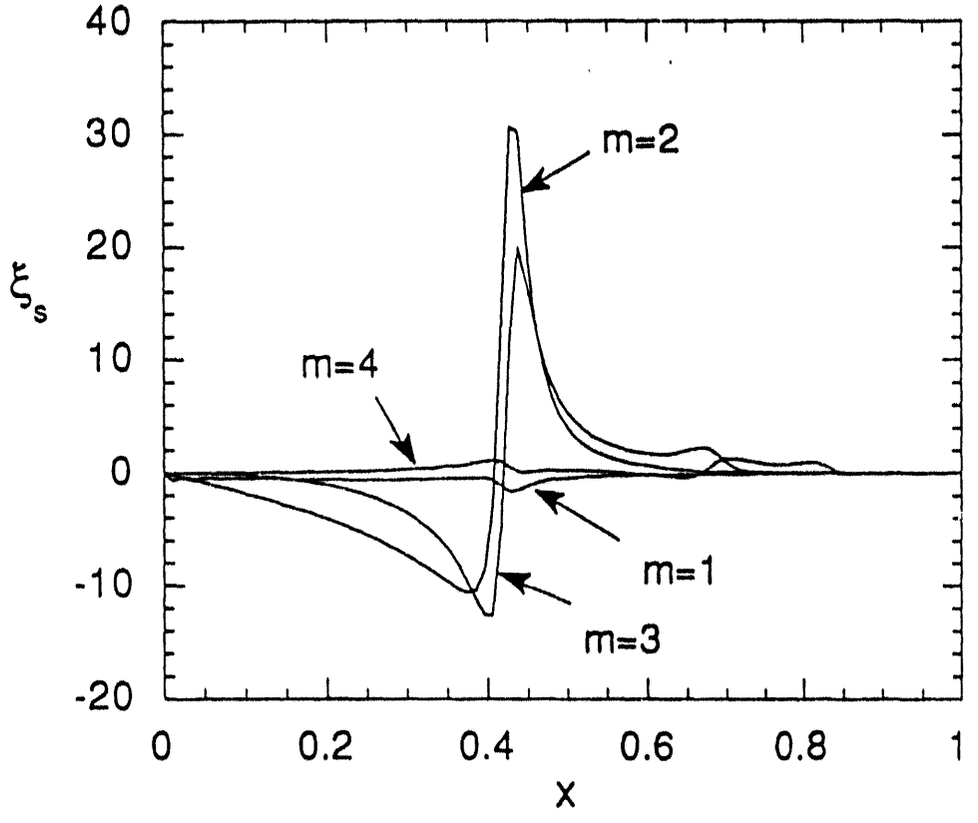

Fig. 1

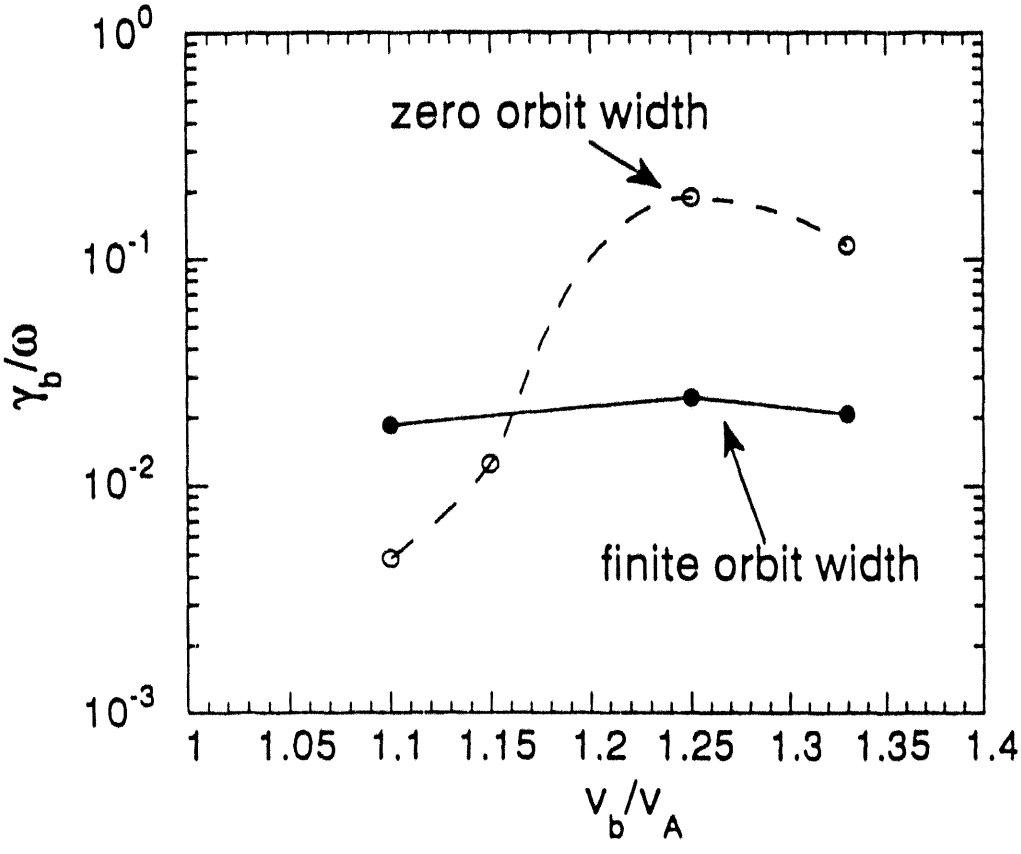
10^0
10^{-1}
10^{-2}
10^{-3}
γ_b/ω
zero orbit width
finite orbit width
1
1.05
1.1
1.15
1.2
1.25
1.3
1.35
1.4
V_b/V_A

Fig. 2

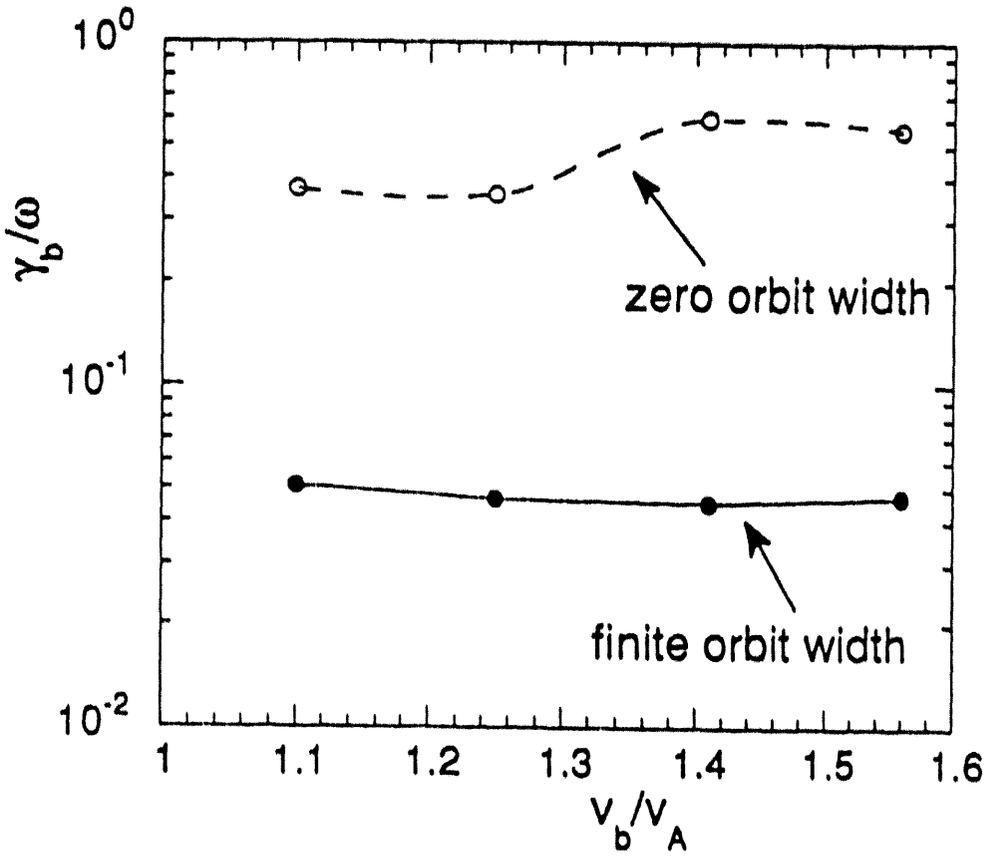
10^0
10^{-1}
10^{-2}
γ_b/ω
zero orbit width
finite orbit width
1
1.1
1.2
1.3
1.4
1.5
1.6
V_b/V_A

Fig. 3

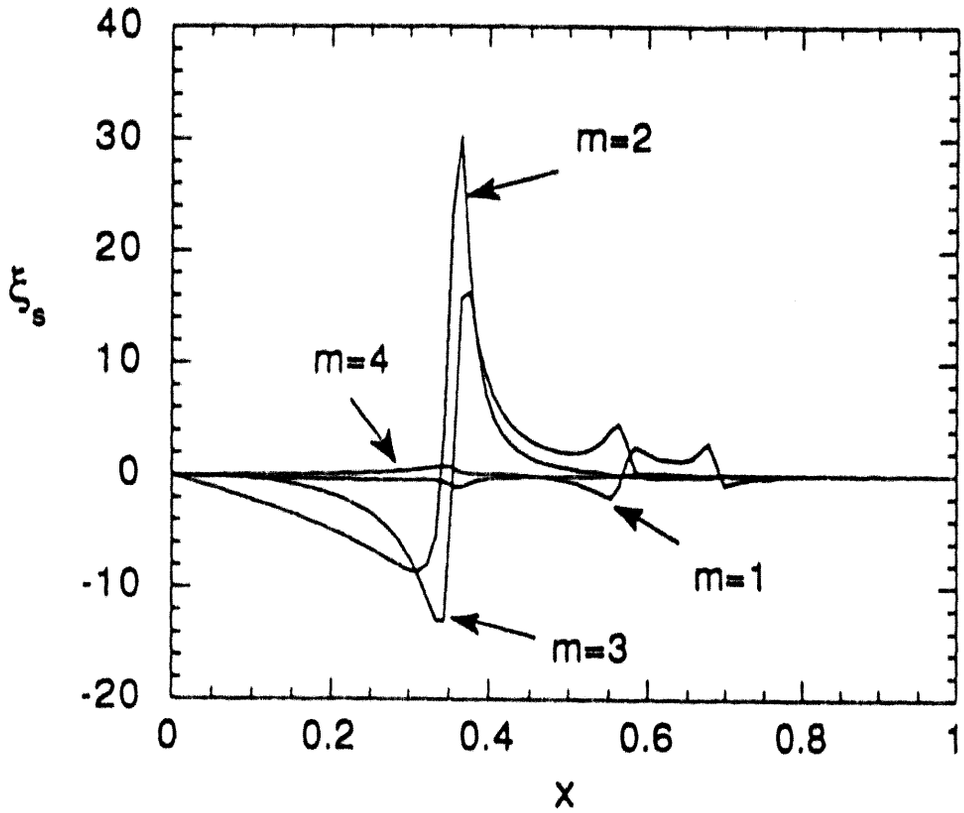

Fig. 4

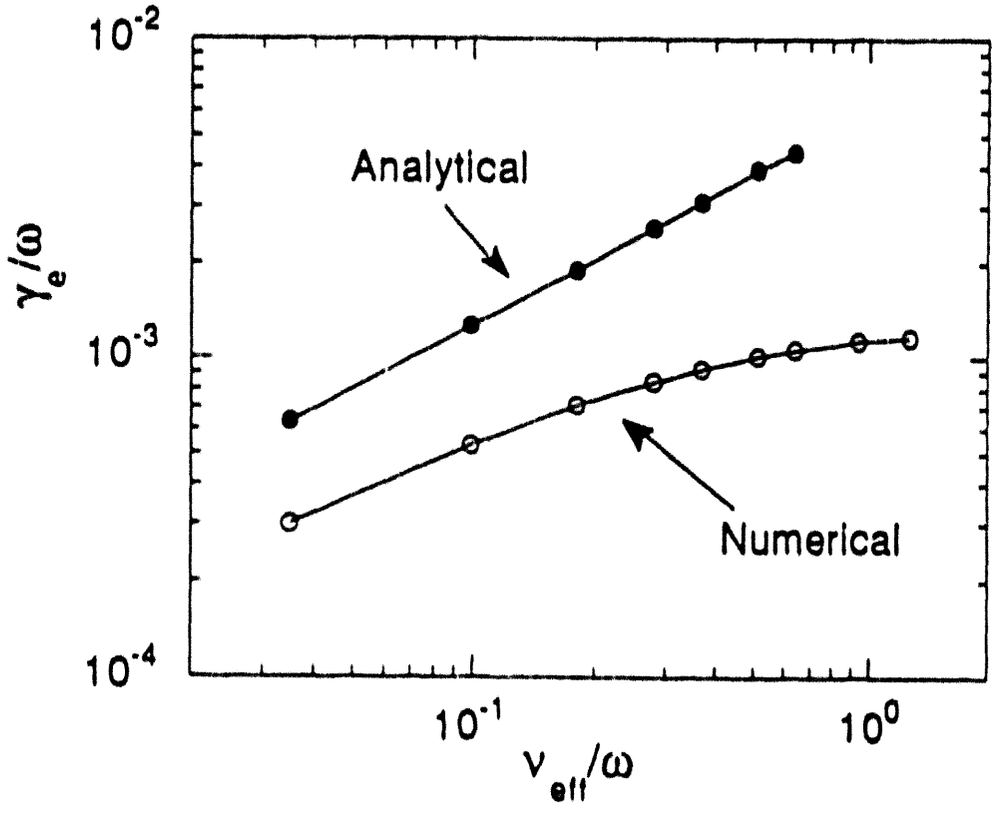
10^{-2}
10^{-3}
10^{-4}
γ_e/ω
Analytical
Numerical
10^{-1}
10^{0}
ν_{eff}/ω

Fig. 5

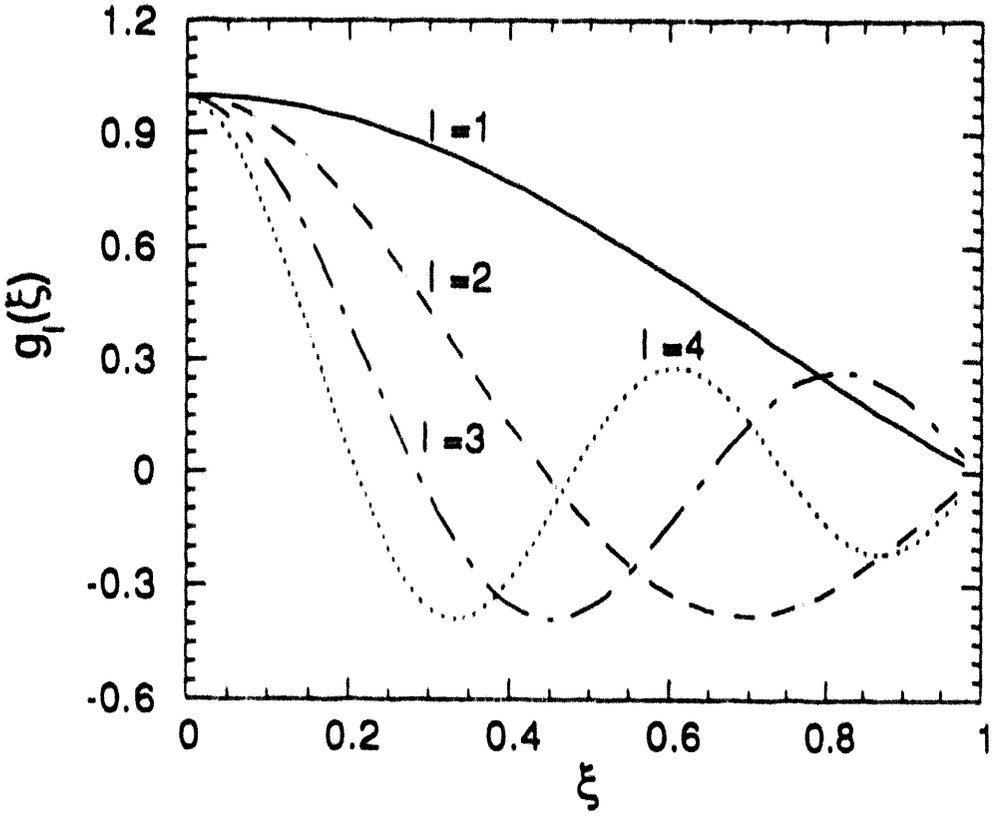

Fig. 6

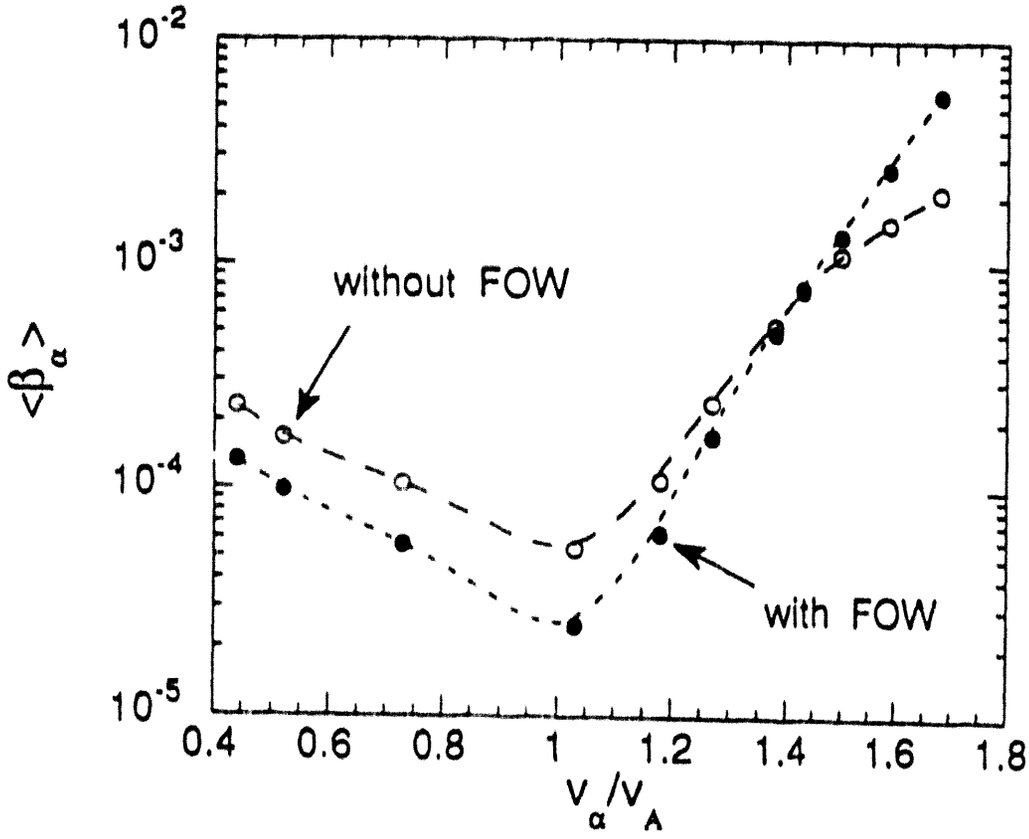
10^{-2}
10^{-3}
10^{-4}
10^{-5}
$<\hat{\beta}_\alpha>$
without FOW
with FOW
0.4
0.6
0.8
1
1.2
1.4
1.6
1.8
V_α/V_A

Fig. 7

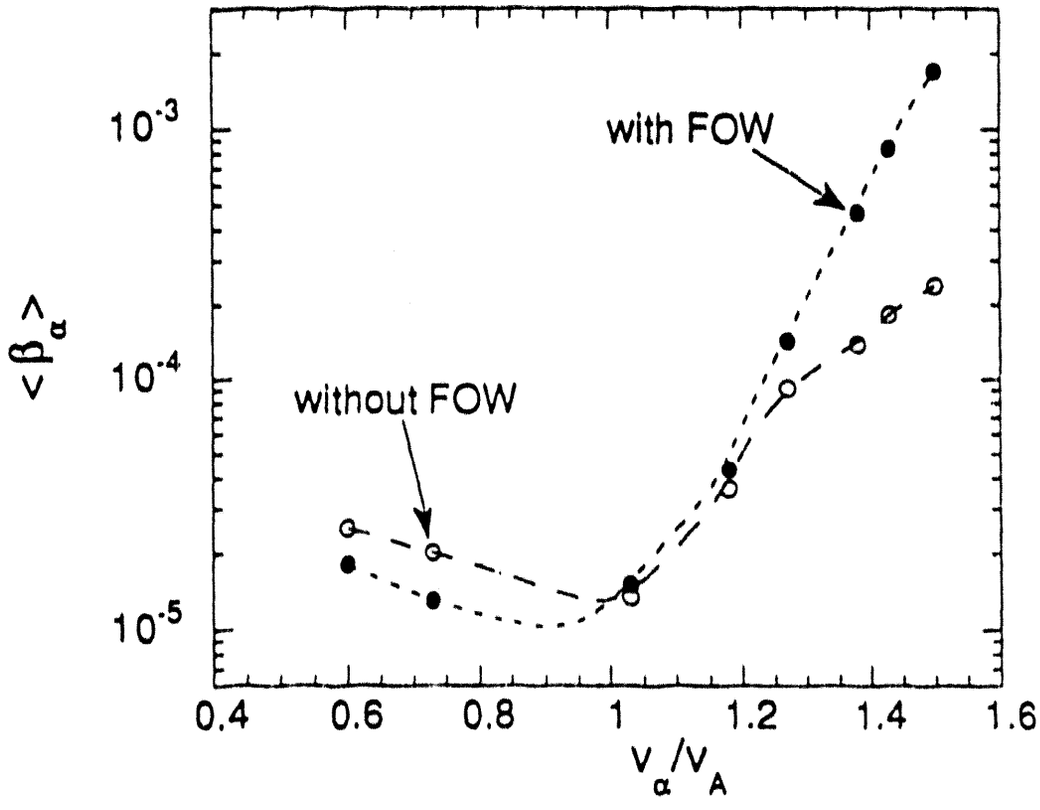
with FOW
without FOW
10^{-3}
10^{-4}
10^{-5}
$\langle \beta_\alpha \rangle$
0.4
0.6
0.8
1
1.2
1.4
1.6
V_α/V_A

Fig. 8

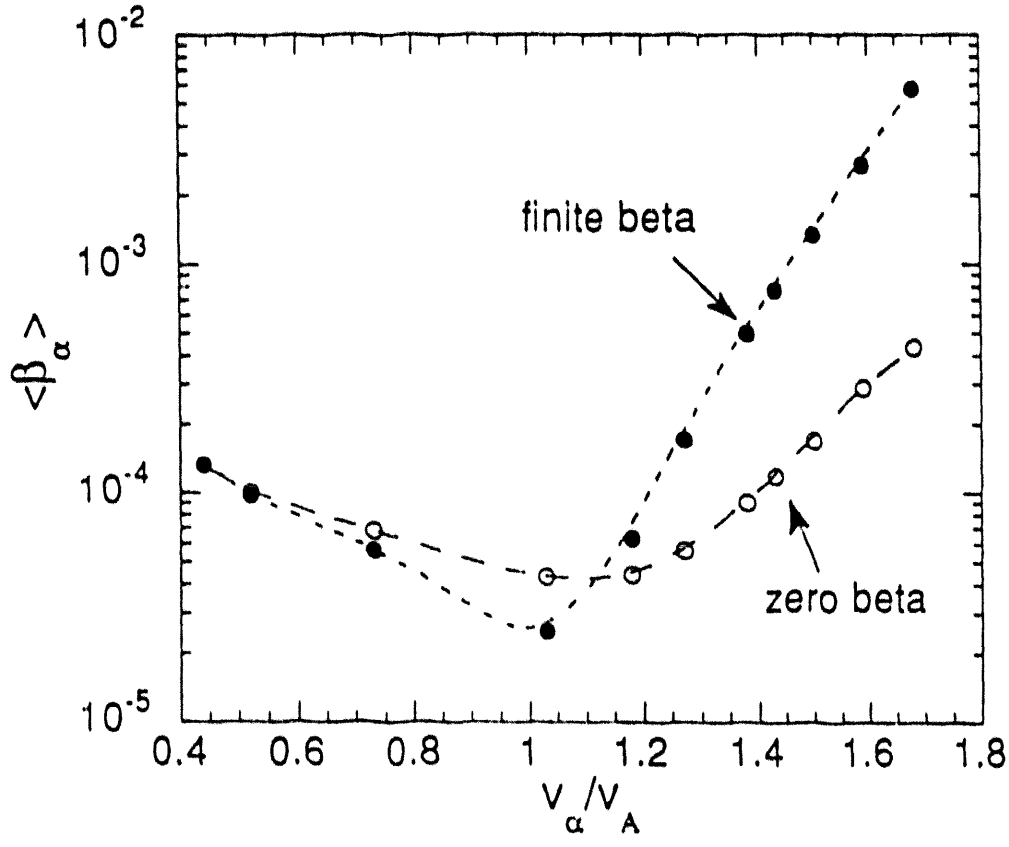
finite beta
zero beta
10^{-2}
10^{-3}
10^{-4}
10^{-5}
$\langle \hat{\beta}_\alpha \rangle$
0.4
0.6
0.8
1
1.2
1.4
1.6
1.8
V_α/V_A

Fig. 9

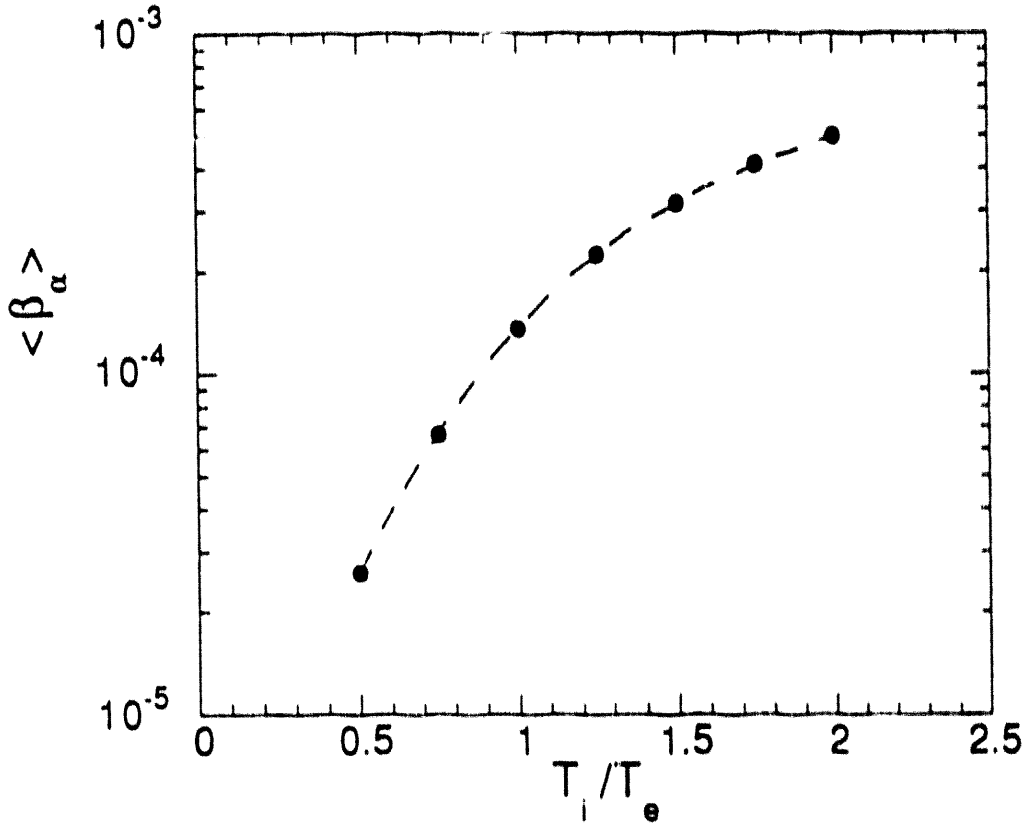

Fig. 10

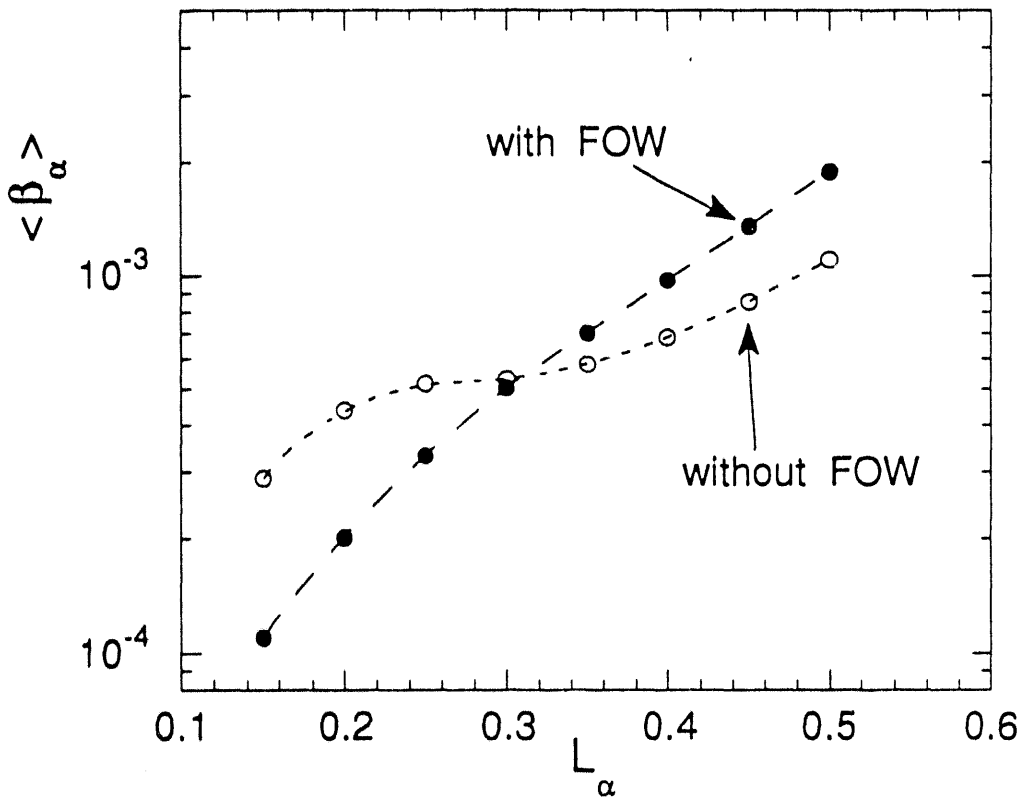
with FOW
without FOW
$<\beta_\alpha>$
10^{-3}
10^{-4}
0.1
0.2
0.3
0.4
0.5
0.6
L_α

Fig. 11

EXTERNAL DISTRIBUTION IN ADDITION TO UC-420

Dr. F. Paoloni, Univ. of Wollongong, AUSTRALIA
Prof. M.H. Brennan, Univ. of Sydney, AUSTRALIA
Plasma Research Lab., Australian Nat. Univ., AUSTRALIA
Prof. I.R. Jones, Flinders Univ, AUSTRALIA
Prof. F. Cap, Inst. for Theoretical Physics, AUSTRIA
Prof. M. Heindler, Institut für Theoretische Physik, AUSTRIA
Prof. M. Goossens, Astronomisch Instituut, BELGIUM
Ecole Royale Militaire, Lab. de Phy. Plasmas, BELGIUM
Commission-European, DG. XII-Fusion Prog., BELGIUM
Prof. R. Boucique, Rijksuniversiteit Gent, BELGIUM
Dr. P.H. Sakanaka, Instituto Fisica, BRAZIL
Instituto Nacional De Pesquisas Espaciais-INPE, BRAZIL
Documents Office, Atomic Energy of Canada Ltd., CANADA
Dr. M.P. Bachynski, MPB Technologies, Inc., CANADA
Dr. H.M. Skarsgard, Univ. of Saskatchewan, CANADA
Prof. J. Teichmann, Univ. of Montreal, CANADA
Prof. S.R. Sreenivasan, Univ. of Calgary, CANADA
Prof. T.W. Johnston, INRS-Energie, CANADA
Dr. R. Bolton, Centre canadien de fusion magnétique, CANADA
Dr. C.R. James,, Univ. of Alberta, CANADA
Dr. P. Lukác, Komenského Universzita, CZECHO-SLOVAKIA
The Librarian, Culham Laboratory, ENGLAND
Library, R61, Rutherford Appleton Laboratory, ENGLAND
Mrs. S.A. Hutchinson, JET Library, ENGLAND
Dr. S.C. Sharma, Univ. of South Pacific, FIJI ISLANDS
P. Mähönen, Univ. of Helsinki, FINLAND
Prof. M.N. Bussac, Ecole Polytechnique,, FRANCE
C. Mouttet, Lab. de Physique des Milieux Ionisés, FRANCE
J. Radet, CEN/CADARACHE - Bat 506, FRANCE
Prof. E. Economou, Univ. of Crete, GREECE
Ms. C. Rinni, Univ. of Ioannina, GREECE
Dr. T. Mual, Academy Bibliographic Ser., HONG KONG
Preprint Library, Hungarian Academy of Sci., HUNGARY
Dr. B. DasGupta, Saha Inst. of Nuclear Physics, INDIA
Dr. P. Kaw, Inst. for Plasma Research, INDIA
Dr. P. Rosenau, Israel Inst. of Technology, ISRAEL
Librarian, International Center for Theo. Physics, ITALY
Miss C. De Palo, Associazione EURATOM-ENEA, ITALY
Dr. G. Grosso, Istituto di Fisica del Plasma, ITALY
Prof. G. Rostangni, Istituto Gas Ionizzati Del Cnr, ITALY
Dr. H. Yamato, Toshiba Res. & Devel. Center, JAPAN
Prof. I. Kawakami, Hiroshima Univ., JAPAN
Prof. K. Nishikawa, Hiroshima Univ., JAPAN
Director, Japan Atomic Energy Research Inst., JAPAN
Prof. S. Itoh, Kyushu Univ., JAPAN
Research Info. Ctr., National Instit. for Fusion Science, JAPAN
Prof. S. Tanaka, Kyoto Univ., JAPAN
Library, Kyoto Univ., JAPAN
Prof. N. Inoue, Univ. of Tokyo, JAPAN
Secretary, Plasma Section, Electrotechnical Lab., JAPAN
S. Mori, Technical Advisor, JAERI, JAPAN
Dr. O. Mitarai, Kumamoto Inst. of Technology, JAPAN
J. Hyeon-Sook, Korea Atomic Energy Research Inst., KOREA
D.I. Choi, The Korea Adv. Inst. of Sci. & Tech., KOREA
Prof. B.S. Liley, Univ. of Waikato, NEW ZEALAND
Inst of Physics, Chinese Acad Sci PEOPLE'S REP. OF CHINA
Library, Inst. of Plasma Physics, PEOPLE'S REP. OF CHINA
Tsinghua Univ. Library, PEOPLE'S REPUBLIC OF CHINA
Z. Li, S.W. Inst. Physics, PEOPLE'S REPUBLIC OF CHINA
Prof. J.A.C. Cabral, Instituto Superior Tecnico, PORTUGAL
Dr. O. Petrus, AL.I. CUZA Univ., ROMANIA
Dr. J. de Villiers, Fusion Studies, AEC, S. AFRICA
Prof. M.A. Hellberg, Univ. of Natal, S. AFRICA
Prof. D.E. Kim, Pohang Inst. of Sci. & Tech., SO. KOREA
Prof. C.I.E.M.A.T, Fusion Division Library, SPAIN
Dr. L. Stenflo, Univ. of UMEA, SWEDEN
Library, Royal Inst. of Technology, SWEDEN
Prof. H. Wilhelmson, Chalmers Univ. of Tech., SWEDEN
Centre Phys. Des Plasmas, Ecole Polytech, SWITZERLAND
Bibliotheek, Inst. Voor Plasma-Fysica, THE NETHERLANDS
Asst. Prof. Dr. S. Cakir, Middle East Tech. Univ., TURKEY
Dr. V.A. Glukhikh, Sci. Res. Inst. Electrophys.I Apparatus, USSR
Dr. D.D. Ryutov, Siberian Branch of Academy of Sci., USSR
Dr. G.A. Eliseev, I.V. Kurchatov Inst., USSR
Librarian, The Ukr.SSR Academy of Sciences, USSR
Dr. L.M. Kovrizhnykh, Inst. of General Physics, USSR
Kernforschungsanlage GmbH, Zentralbibliothek, W. GERMANY
Bibliothek, Inst. Für Plasmaforschung, W. GERMANY
Prof. K. Schindler, Ruhr-Universität Bochum, W. GERMANY
Dr. F. Wagner, (ASDEX), Max-Planck-Institut, W. GERMANY
Librarian, Max-Planck-Institut, W. GERMANY
Prof. R.K. Janev, Inst. of Physics, YUGOSLAVIA

DATE
FILMED
11/22/93

END